Technical Note

Effect of Pore–Fluid Chemistry on the Undrained Shear Strength of Xanthan Gum Biopolymer-Treated Clays

Ilhan Chang, Ph.D., A.M.ASCE[1]; Yeong-Man Kwon[2]; and Gye-Chun Cho, Ph.D.[3]

Abstract: Xanthan gum (XG) biopolymer-based soil treatment is an effective soil improvement method. In this study, we explored the effect of XG on the undrained shear strength of clays (kaolinite and montmorillonite) in chemically distinct pore fluids. Among the pore fluids tested, the undrained shear strength of kaolinite was the highest in kerosene, followed by deionized (DI) water and brine. This study hypothesized that the interparticle forces and interactions dominated the undrained shear strength of the kaolinite clay. In contrast, montmorillonite showed the highest undrained shear strength with DI water, followed by brine and kerosene, likely due to the increase in thickness of the viscous double layer that reduced the undrained strength of the montmorillonite clay. XG also affected the undrained shear strength of the clays, possibly due to the increase in viscosity of the pore fluids and modification of the clay interparticle fabrics. In DI water, XG increased the undrained shear strength of kaolinite (maximum shear strength was observed in the sample with an XG-to-soil mass ratio of 0.5%) via water absorption. Simultaneously, XG decreased the undrained shear strength of montmorillonite, likely due to XG-induced particle aggregation resulting from the changes in the montmorillonite particle surface charges. In 2-M-NaCl brine, the undrained shear strength increased with the increase in XG content, regardless of the mineral types, owing to the salt-induced double-layer compression and increase in concurrent XG-induced pore–fluid viscosity. However, the unaffected and constant undrained shear strength of both clays in nonpolar kerosene suggests that hydrating XG is a prerequisite for its application in soil treatment. **DOI: 10.1061/(ASCE)GT.1943-5606.0002652.**

Author keywords: Xanthan gum (XG); Biopolymer; Clay; Pore–fluid chemistry; Undrained shear strength; Kaolinite; Montmorillonite; Fall cone test; Soil stabilization.

Introduction

Undrained shear strength (s_u) is an important geotechnical engineering design parameter for clayey soils in undrained conditions (e.g., submarine, offshore, glacial, and deep sediments), which is generally assessed by high shear rates and poor drainage conditions (Gutierrez et al. 2008; Kayabali and Tufenkci 2010). Despite several factors affecting the s_u of clays, the net derjaguin-landau-verwey-overbeek (DLVO) forces between clay particles (Warkentin and Yong 1962) and pore (or double-layer) fluid chemistry (Sridharan and Prakash 1999) are important factors affecting the s_u of clays.

Factors influencing the net DLVO forces among clays include clay mineralogy, plasticity, fabrics, pore–fluid chemistry, water content, stress history, anisotropy, and organics (Mayne 1985; Hyde and Ward 1986; Dolinar and Trauner 2007; Kayabali and Tufenkci 2010; Spagnoli et al. 2010; Hong et al. 2013). The net DLVO forces change the particle associations, thereby affecting the s_u of clays; the edge-to-face associations show higher s_u compared to other types of associations (i.e., edge-to-edge and face-to-face) because the Coulombic attraction between the oppositely charged edge and the face surface is significantly stronger than their van der Waals attraction (Dolinar and Trauner 2007). Furthermore, the collapse and reorientation of the edge-to-face contact result in a denser and more stable local geometry (Sachan and Penumadu 2007).

Pore–fluid chemistry can alter particle arrangements (e.g., flocculation and deflocculation); thus, it plays an important role in the s_u of clays. For example, salinity conditions affect the shear strength of soils, which experiences frequent changes in salinity due to freshwater or saltwater mixing (Schlue et al. 2010). Furthermore, the s_u of clays increases as the particle grain size decreases (i.e., the specific surface area increases) due to the larger water absorption capacity (Trauner et al. 2005).

Microbial biopolymers are polymeric biomolecules that are produced through the metabolism of microorganisms. Biopolymers contain side chains (e.g., trisaccharide) that can interact with charged clay particles, counterions, and pore water through hydrogen bonding (Chenu and Guérif 1991; Chang and Cho 2019; Chang et al. 2019). Thus, biopolymers have been reported as effective and ecofriendly soil modification materials owing to their ability to clog pore spaces (Khachatoorian et al. 2003; Bouazza et al. 2009; Chang et al. 2016a; Lee et al. 2019; Zhou et al. 2020) and enhance interparticle bonding between soil particles (Malik and Letey 1991; Kwon et al. 2017; Latifi et al. 2017; Chang et al. 2020; Soldo et al. 2020; Sujatha et al. 2020). Moreover, biopolymers have been shown to form viscous hydrogels and interact with the charged surfaces of clays (Chang et al. 2015, 2020). For instance, Sujatha et al. (2020) showed that xanthan gum (XG) biopolymer forms an interconnected network between the biopolymer molecules and soil surface, which results in a decrease in permeability and increase in strength. The interconnected network also

[1]Associate Professor, Dept. of Civil Systems Engineering, Ajou Univ., Suwon-si 16499, Republic of Korea. ORCID: https://orcid.org/0000-0001-8369-0606. Email: ilhanchang@ajou.ac.kr

[2]Graduate Student, Dept. of Civil and Environmental Engineering, Korea Advanced Institute of Science and Technology, Daejeon 34141, Republic of Korea. ORCID: https://orcid.org/0000-0002-4719-1241. Email: yeongman.kwon@kaist.ac.kr

[3]Professor, Dept. of Civil and Environmental Engineering, Korea Advanced Institute of Science and Technology, Daejeon 34141, Republic of Korea (corresponding author). Email: gyechun@kaist.edu

Note. This manuscript was submitted on March 10, 2020; approved on June 25, 2021; published online on August 27, 2021. Discussion period open until January 27, 2022; separate discussions must be submitted for individual papers. This technical note is part of the ***Journal of Geotechnical and Geoenvironmental Engineering***, © ASCE, ISSN 1090-0241.

Table 1. Index properties of the clays that were used in this study

Type of clay	D_{50} (μm)	SSA (m^2/g)[a]	CEC (meq/100 g)[b]	pH[c]	XG (%)	Deionized water		2 M NaCl		Kerosene	
						PL (%)	LL (%)	PL (%)	LL (%)	PL (%)	LL (%)
Kaolinite	3	22	6.1	4.2	0	31	70	34	51	—	93
					0.1	35	74	36	52		93
					0.5	32	97	37	55		91
					1	40	80	33	61		84
					2	36	79	46	71		92
Montmorillonite[d]	0.07	221	64.1	6.5	0	62	389	42	86	—	61
					0.1	54	386	46	96		60
					0.5	55	373	44	100		60
					1	71	370	43	106		58
					2	69	338	41	114		59

[a]Specific surface area obtained by the methylene blue adsorption measurement (Santamarina et al. 2002).
[b]Cation exchange capacity measured using the methylene blue cation exchange capacity (Inglethorpe et al. 1993).
[c]Supernatant pH measured after settling sediment with 300% water content.
[d]The chemical composition of the original montmorillonite is SiO_2, Al_2O_3, Fe_2O_3, CaO, MgO, TiO_2, Na_2O, and K_2O and loss of ignition (Anirudhan and Ramachandran 2007).

resists compaction, resulting in a lower maximum dry density and higher optimal moisture content (Dehghan et al. 2019).

In addition, biopolymer-based soil treatments have been shown to significantly enhance the hydraulic erosion resistance of soils (Ham et al. 2018; Kwon et al. 2020), which is expected to effectively mitigate erosion or scouring problems of waterfront geotechnical engineering structures. Additional studies showed that biopolymer-induced soil flocculation accelerates the settling velocity and reduces the turbidity of soil suspensions (Kwon et al. 2017; Kang and McLaughlin 2020), which is useful for sludge dewatering (Guo and Wen 2020). Meanwhile, the redistribution of XG (i.e., from strong intergranular bridges to a uniform distribution around the grains) occurs during the wetting–drying cycles, which gradually reduces the overall shear strengthening effect of the biopolymer (Chen et al. 2019a). Singh and Das (2020) showed that biopolymer treatment reduces mass loss during repeated freeze–thaw cycles.

Biopolymer interactions with pore fluids and clay particles can improve the shear strength of soils, accompanied by an increase in the friction angle or cohesion (Khatami and O'Kelly 2012; Chang and Cho 2019; Chen et al. 2019b) via particle aggregation and the following conglomeration effect (Chang and Cho 2019); this would improve the erosion resistance of fine-grained soils (Ham et al. 2018; Kwon et al. 2020). However, the effect of the pore–fluid chemistry on the s_u of biopolymer-treated clays has not yet been investigated.

In this study, we explored the effect of the XG content, clay mineralogy, and pore–fluid type (deionized [DI] water, 2-M-NaCl brine, and kerosene) on the s_u of kaolinite and montmorillonite clays. The s_u of the XG-treated soils with different pore–fluid types and contents was evaluated through fall cone tests. The morphology of the clay particles in the presence of different pore fluids, ions, and XG was analyzed using scanning electron microscopy (SEM).

Materials and Methods

Characteristics of the Clay Materials

Kaolinite (1:1 type; Bintang, Indonesia) and montmorillonite (2:1 type, CAS: 1302-78-9; Sigma-Aldrich, Bellefonte, Pennsylvania) were used to examine and compare the effects of clay mineralogy on the s_u. Kaolinite has low swelling and reactive areas on its external surfaces because the basal oxygen atoms of the tetrahedral silica sheet and the hydroxyls of the octahedral alumina sheet are held together by hydrogen bonding (Giese 2003). Meanwhile, montmorillonite shows a high swelling potential upon water addition because its layers are loosely held together by van der Waals forces (Chen and Peng 2018).

Although kaolinite presents a larger particle size than montmorillonite, the latter exhibits a higher specific surface area (SSA), cation exchange capacity (CEC), and a thicker double layer, as shown in Table 1. Kaolinite presents a lower aspect ratio and a higher positive edge charge portion (Tombácz and Szekeres 2006; Villanueva et al. 2010), whereas montmorillonite contains approximately 90%–95% of pH-insensitive negative charges contributing to the total charge (Au and Leong 2016). Thus, the attraction between the edge and face charges is more critical to the s_u of kaolinite than in montmorillonite (Penner and Lagaly 2001).

Montmorillonite clays have more negative zeta potential (i.e., the potential difference between the media and clay layers) than kaolinite minerals because they have more SiO^- groups on their surface, owing to their 2:1 structure (Doi et al. 2019). When salt (e.g., Na- or Cs-halide) is added, the negative zeta potential of kaolinite tends to be more negative owing to the formation of pH-dependent groups (Liu et al. 2012), whereas that of montmorillonite becomes neutralized by cation adsorption owing to the enhanced interlayer activity (Doi et al. 2019).

Prior to the experiments, kaolinite was washed six times with DI water to remove the supernatants after solid and fluid separation (Wang and Siu 2006), whereas montmorillonite was used without washing. The clays were dried in an oven (110°C) according to ASTM D2216-19 (ASTM 2019). The index properties of the clays used are listed in Table 1.

Characteristics of Xanthan Gum

XG is a biopolymer produced by *Xanthomonas campestris*; its structure consists of repeating glucose units and side chains with three sugar units (García-Ochoa et al. 2000). XG is water soluble, and once dissolved, its structure expands, and the side chains that consist of glucuronic and pyruvic acid groups become negatively charged (Hassler and Doherty 1990; Nugent et al. 2009; Petri 2015). Therefore, XG is widely used as a thickener and stabilizer for suspensions, solid particles, and foams in aqueous formulations (Katzbauer 1998; Chang et al. 2016b). XG has shown high potential

for soil stabilization through the enhancement of its shear strength (Lee et al. 2017; Chang and Cho 2019) and compressive strength (Kwon et al. 2019) via clay–XG aggregation (Chang et al. 2019). Moreover, XG reduces the hydraulic conductivity of soil owing to pore clogging induced by XG hydrogels (Cabalar et al. 2017). A research-grade XG (CAS: 11138-66-2; Sigma-Aldrich, Saint Louis) was used in this study for the experiments.

Preparation of the XG–Clay Mixture

Washed and oven-dried clays were mixed with XG powder at mass ratios (m_b/m_s) of 0% (untreated), 0.1%, 0.5%, 1.0%, and 2.0%. Three chemically distinct pore fluids, namely DI water, 2-M-NaCl brine (high ionic concentration), and kerosene (low permittivity), were used, as in previous studies (Jang and Santamarina 2016; Cao et al. 2019). XG solutions were prepared by mixing these pore fluids with dry XG powder. Oven-dried clays and XG solutions were mixed until the formation of uniform XG–clay-pore fluid mixtures. We prepared 2-M-NaCl brine (i.e., two moles of NaCl per liter of DI water) by dissolving 58.44 g (1 mol) of NaCl (CAS No. 1310-58-3; Junsei Chemical Co., Tokyo) in 500 mL of DI water in a beaker using a magnetic stirrer to form 500 mL of a uniform 2-M-NaCl solution. During the experimental procedures, the fluid-to-dry soil ratio ($w = m_w/m_s$) was adjusted by adding the prepared pore fluids into the soils at gradual increments and thoroughly mixed using a laboratory spatula to obtain uniform soil samples. The liquid limit (LL) and plastic limit (PL) of the XG–clay mixtures in Table 1 were measured via laboratory fall cone tests (British Standards Institution 2017) and the thread rolling method (ASTM 2017), respectively.

Experimental Details and Testing Procedure

The s_u of clay was evaluated via laboratory fall cone tests (Wood 1990; Koumoto and Houlsby 2001; O'Kelly et al. 2018). The effect of the shearing rate on the s_u values obtained from the fall cone tests was not investigated in this study; however, differences in the shearing rates may have existed between the fall cone tests and could have nonnegligible influences on the obtained s_u values. Koumoto and Houlsby (2001) analyzed the strain effect on s_u by comparing laboratory triaxial test and fall cone test measurements; s_u was reported to have increased by 60% at high strain rates. Kulhawy and Mayne (1990) analyzed the triaxial compression data and observed a 10% increase in s_u per log cycle of the strain rate. In contrast, Chow et al. (2012) argued that the s_u measured with parallel plate rotational viscometer tests was smaller than that assessed using conventional triaxial tests owing to the viscous rate effect.

In this study, XG–clay mixtures were tamped into a container with a 55-mm diameter and 40-mm height. Soils with a degree of saturation higher than 90% were used. After surface trimming, the wet weight was measured to obtain the density information (e.g., dry density, total density, and void ratio) for each specimen. Simultaneously, a cone penetration test was conducted to prevent alterations in the specimen moisture contents. The 80-g and 30°-apex cone could penetrate the soil pastes for 5 sec. The s_u of the clay obtained from the fall cone test (s_u^{FC}) was calculated as follows:

$$s_u^{FC} = K\frac{w}{d^2} \tag{1}$$

where K = cone factor that reflects the friction effect between the cone and soil (Stone and Phan 1995); W = weight of the cone (80 g); and d = cone penetration depth (mm). A K value of 0.867 was adopted for the 30°-apex cone, which corresponds to $s_u^{LL} = 1.7$ kPa (s_u^{LL} is the s_u when $w = LL$) (Sharma and Bora Padma 2003; Kayabali and Tufenkci 2010). The s_u values of the soils with liquidity index [$LI = (w - PL)/(LL - PL)$] values greater than 0.2 were measured to avoid potential overestimations (Vardanega and Haigh 2014).

A laboratory vane shear test was performed simultaneously on untreated clays under the same conditions to obtain the vane shear strength (s_u^V) of untreated clays for comparison and verification. This was achieved using a rectangular vane (width = 12.7 mm, height = 12.7 mm, and thickness = 0.05 mm) with a rotation velocity of 60°/min according to ASTM D4648/D4648M-16 (ASTM 2016). For each XG–clay–water content (w) condition, fall cone and vane shear tests were conducted with three different specimens to obtain reliable average values for s_u^{FC} and s_u^V. After the measurements, the XG–clay-pore fluid samples around the cone and vane intrusion were collected and dried in an oven at 110°C for 24 h to obtain the w following ASTM D2216-19 (ASTM 2019).

The microstructures of the clays (untreated and XG-treated) were observed using SEM (S-4800 and SU-8230, Hitachi High Technologies, Tokyo). The clays were sampled at $w = LL$. The samples were air-dried at room temperature and attached to a 25-mm-diameter SEM mount with carbon conductive tabs (Pelco Tabs; Ted Pella, Redding, California). The specimens were coated with osmium (OsO_4) for 10 s under vacuum using a plasma coater (OPC-60A). Conventional SEM was conducted to observe the morphology in terms of the effect of XG and pore fluids on the clays. However, advanced microscopy techniques, such as environmental-SEM (Carrier et al. 2013) or cryo-SEM (Du et al. 2009), are needed to analyze the XG–clay–salt water interactions in moist conditions.

Correlations between s_u and Index Properties

Koumoto and Houlsby (2001) suggested the following linear regression equation showing the relationship between log s_u and log w:

$$s_u = \left(\frac{w}{\alpha}\right)^{-\frac{1}{\beta}} \tag{2}$$

where α = water content when s_u is 1 kPa; and β = slope of log w and log s_u. In addition, α and β depend on the soil plasticity, compressibility, SSA, particle structure, pore–fluid chemistry, and organic matter content (Koumoto and Houlsby 2001; Trauner et al. 2005; Dolinar and Trauner 2007).

From Eqs. (1) and (2), s_u and LI can be correlated as follows (Wroth and Wood 1978; Wood 1990):

$$s_u = s_u^{LL} R^{(1-LI)} \tag{3}$$

where s_u^{LL} = undrained shear strength at LL; and R = ratio between the s_u values at PL and LL. The R factor value depends on the clay mineral type and soil activity (Wood 1990). The correlation factors (α, β, and R) can be used to estimate the s_u of the clays, with w and the index properties (e.g., LL, LI) assessed in the laboratory.

Results and Analyses

Effect of Pore–Fluid Chemistry on the $s_u - w$ Relationship

This study investigated the differences in clay behaviors between water-based (DI water and 2-M-NaCl brine) and kerosene-based mixtures. In clay, the relative permittivity of the pore fluids affects the double-layer forces and accompanying clay fabrics (Espinoza and Santamarina 2012); moreover, the double-layer thickness increases with the relative permittivity of the pore fluids (Mitchell and Soga 2005). However, the van der Waals attraction forces

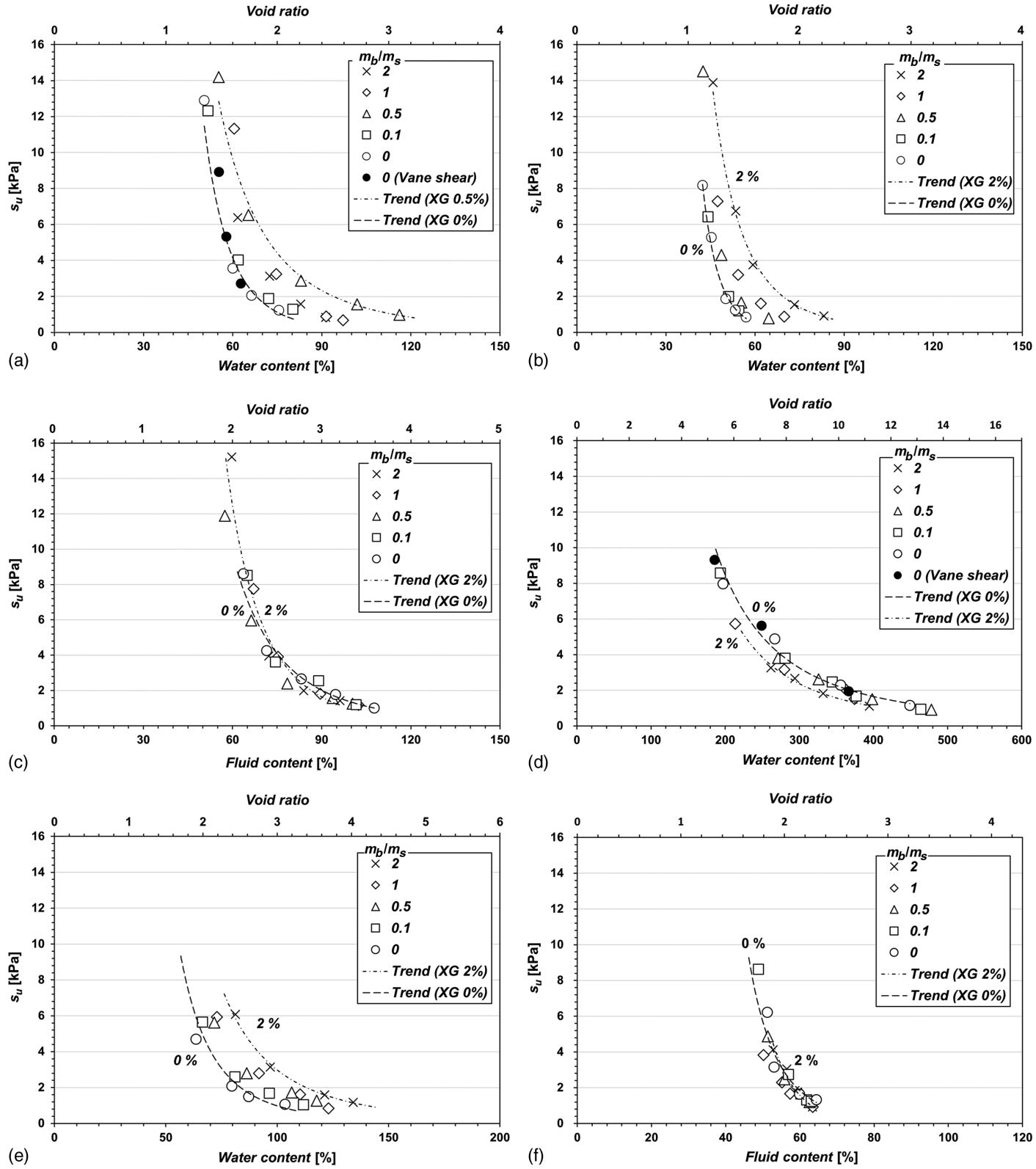

Fig. 1. Variation of s_u in (a, b, and c) kaolinite; and (d, e, and f) montmorillonite with water content and m_b/m_s variation in (a and d) deionized water; (b and e) 2 M NaCl brine; and (c and f) and kerosene. Hollow symbols indicate s_u^{FC} (undrained shear strength from fall cone test), whereas solid symbols indicate s_u^V (undrained shear strength from the vane shear test) of the untreated clays with the deionized water.

related to the Hamaker constant decrease with an increasing pore–fluid relative permittivity (Sridharan and Rao 1979).

Fig. 1 shows the $s_u - w$ relationship for the different clay types and pore fluids, and Fig. 2 presents the α and β variations of the XG-treated clays in terms of the pore–fluid relative permittivity variation based on the data from Fig. 1. The similar trends shown by s_u^V and s_u^{FC} for untreated clays with DI water [Figs. 1(a and d)] validate the fall cone tests conducted to assess the s_u of the clays.

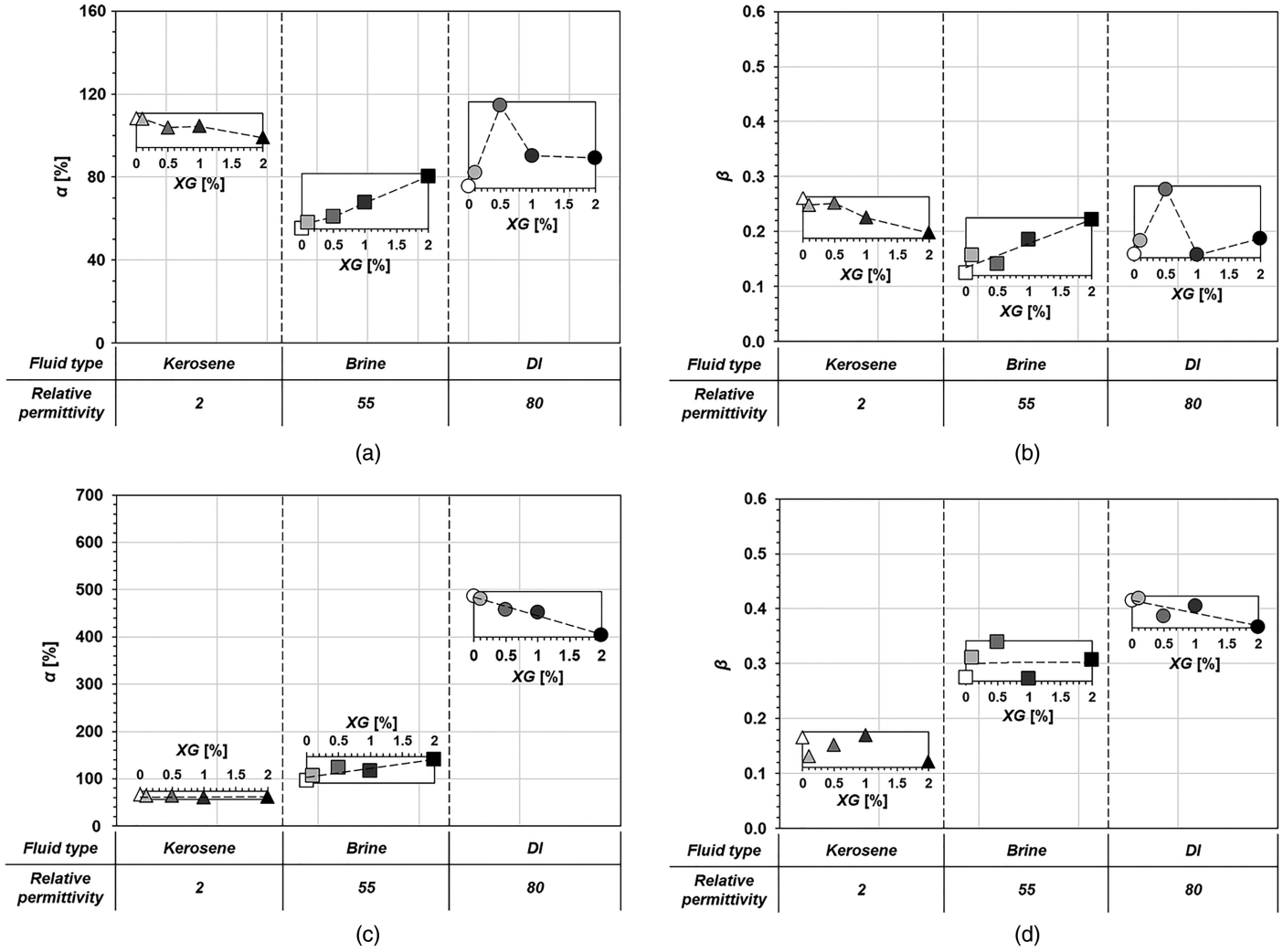

Fig. 2. Variations of the parameters (a and c) α; and (b and d) β with the relative permittivity of the pore fluids and xanthan gum content. The triangle symbols represent soils with kerosene. The rectangular and circular symbols are soils with 2 M NaCl brine and deionized water, respectively. The symbol colors darken from white to black as the xanthan gum content increases.

The s_u of kaolinite is affected by the net attractive forces between the clay particles, whereas that of montmorillonite is affected by the viscous resistance of the double layer (Sridharan and Prakash 1999). Among the different pore fluids, kaolinite shows the highest s_u [Figs. 1(a–c)] and highest α and β values [Figs. 2(a and b)] with kerosene, followed by DI water and brine, whereas montmorillonite shows the highest s_u with DI water, followed by brine and kerosene [Figs. 1(d–f) and 2(c and d)]. Generally, the attraction forces and particle fabrics govern the s_u of kaolinite (Warkentin and Yong 1962; Sridharan and Prakash 1999). Thus, kaolinite exhibited the highest s_u and shear parameters in kerosene, which has the lowest relative permittivity among the three pore fluids. This was due to the presence of edge charges and van der Waals forces, which induced interparticle interactions and consequently increased the s_u of kaolinite (Wang and Siu 2006). Interestingly, various studies have also observed that kaolinite shows an LL increase in nonpolar (low relative permittivity) pore fluids (Jang and Santamarina 2016; Chang et al. 2019).

In contrast, the thick viscous double layers mainly govern the shear resistance of montmorillonite (Warkentin and Yong 1962; Sridharan and Prakash 1999) owing to the high aspect ratio and 2:1 structure of montmorillonite, resulting in low net attraction forces (Secor and Radke 1985; Santamarina et al. 2001; Tombácz and Szekeres 2006). Thus, montmorillonite could have higher s_u [Figs. 1(d–f)], α, and β [Figs. 2(c and d)] values in fluids with higher permittivity.

Effect of Clay Mineralogy on the $s_u - w$ Relationship

While considering the effect of clay mineral type on the s_u, montmorillonite [Fig. 1(d)] required a much higher w than kaolinite [Fig. 1(a)] to achieve the same s_u in DI water owing to the high SSA of montmorillonite; this is in accordance with the findings by Sridharan and Prakash (1999). Because the s_u generally decreases as w increases, montmorillonite shows a higher s_u than kaolinite at the same w.

However, in 2-M-NaCl brine, the salt-induced double-layer suppression and particle rearrangement reduced the shear resistance of both clays (Sridharan and Prakash 1999). Kaolinite [Fig. 1(b)] and montmorillonite [Fig. 1(e)] showed a drastic s_u reduction compared to that in DI water [Figs. 1(a and d) and (2)], whereas montmorillonite had a higher s_u than kaolinite at a similar fluid (2-M NaCl) content. The double-layer compression caused by the cations appeared more prominent for montmorillonite because it presents a

higher CEC and interlayer activity than in kaolinite (Doi et al. 2019).

In the absence of double-layer formation with nonpolar kerosene, kaolinite with a larger edge portion (Wan and Tokunaga 2002) shows higher s_u values than montmorillonite [Figs. 1(c and f) and (2)]. In kerosene, the s_u of the clay is mainly governed by the net attraction forces and fabrics instead of the viscous resistance of the double layers (Jang and Santamarina 2016) because the double-layer thickness of the clay decreases in kerosene (Dukhin and Goetz 2010).

Effect of XG on the $s_u - w$ Relationship

The XG treatment changes the shear resistance of the clays because the net negative charges on the XG branches can interact with the clay particles, salt ions, and water molecules (Chang et al. 2015; Turkoz et al. 2018). Water and salt adsorption by XG increases the s_u of the clays, whereas particle aggregation reduces the s_u owing to the decrease in clay surface area. Thus, kaolinite has more prominent variations in its shear resistance as compared to montmorillonite.

For kaolinite in DI water [Fig. 1(a)], the s_u peaked at $m_b/m_s = 0.5\%$ and decreased at $0.5\% < m_b/m_s < 1\%$. In other words, kaolinite in DI water showed 50% and 70% increments in α and β values with 0.5% of XG, respectively [Figs. 2(a and b)]. A possible hypothesis is that for $m_b/m_s = 0\%$–0.5%, XG mainly absorbs the pore fluids instead of affecting the kaolinite fabrics (Nugent et al. 2009), which increases the pore–fluid viscosity (Milas et al. 1985) and s_u. However, for $0.5\% < m_b/m_s < 1\%$, XG aggregates the kaolinite particles (Nugent et al. 2009) and causes a subsequent decrease in the absorbed water (Chang et al. 2019) and s_u.

In contrast, the maximum s_u of montmorillonite in DI water was observed at $m_b/m_s = 0\%$; subsequently, s_u gradually decreased as m_b/m_s increased [Fig. 1(d)]. With the addition of 2.0% XG, α and β of montmorillonite in DI water decreased by 16% and 11%, respectively [Figs. 2(c and d)]. Because montmorillonite has a higher SSA and CEC than kaolinite, XG could facilitate XG–montmorillonite aggregation while interrupting viscous double-layer formation by montmorillonite particles within DI water (Rao et al. 1993; Laird 1997; Dontsova and Bigham 2005), thereby causing a progressive decrease in s_u with increasing m_b/m_s.

In brine, the s_u of both clays increased with increasing m_b/m_s [Figs. 1(b and e)], which may be attributed to the salt-induced double-layer compression and concurrent XG-induced pore–fluid viscosity increase (Turkoz et al. 2018). Kaolinite showed a 46% increase in α and 74% increase in β, whereas montmorillonite showed increments of 34% and 11% in α and β, respectively (Fig. 2). In contrast, XG has a minor effect on s_u in kerosene, which may be owing to the lack of XG hydration caused by the weak interaction between XG and kerosene (García-Ochoa et al. 2000; Hemar et al. 2001).

Data Reduction Based on the s_u – LI Relationships

The s_u – LI relationships of the XG-treated kaolinite and montmorillonite in DI and 2-M-NaCl brine are presented in Fig. 3; the data

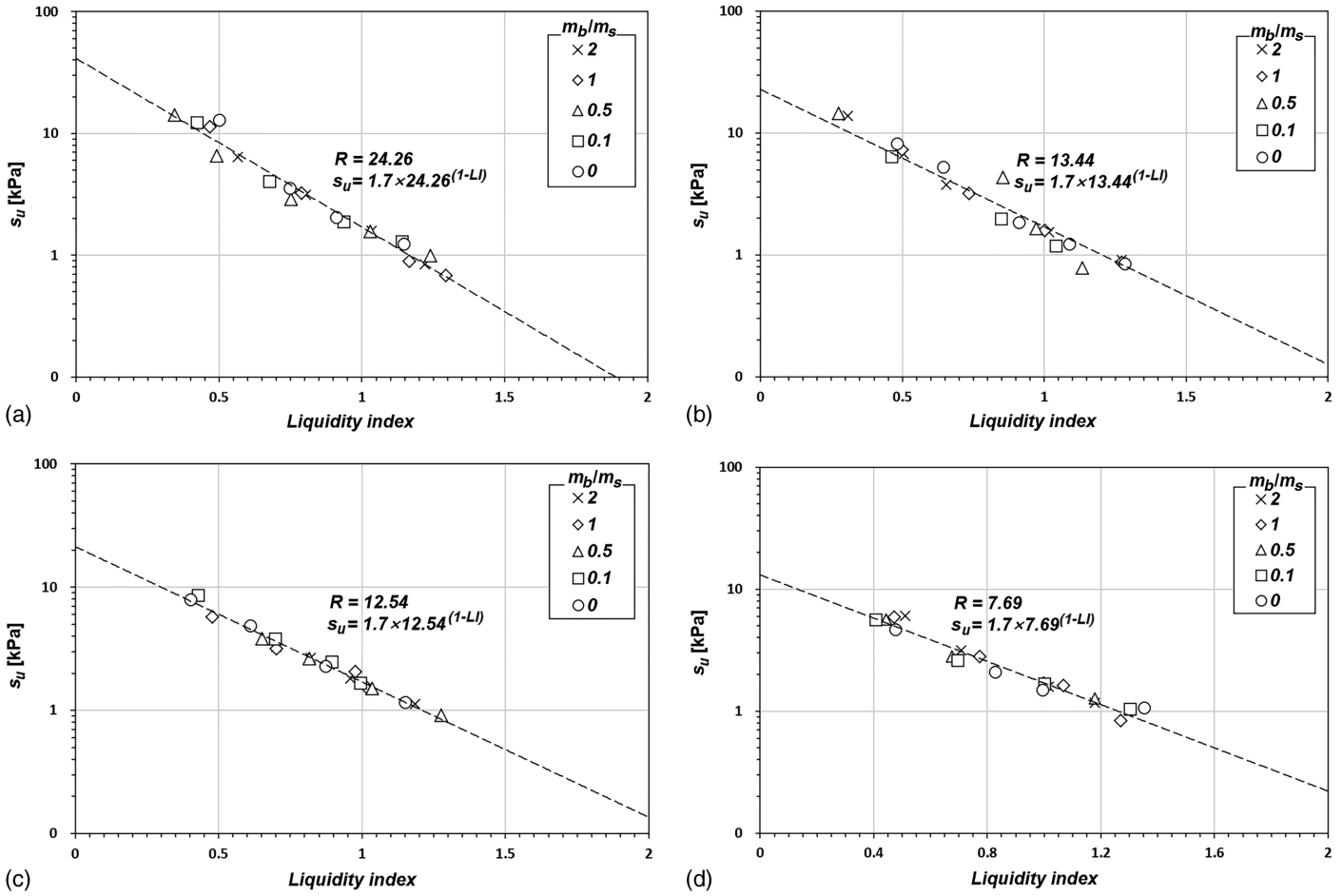

Fig. 3. Variation of s_u with liquidity index for various clays in different pore fluids: (a) kaolinite in deionized water; (b) kaolinite in 2 M NaCl brine; (c) montmorillonite in deionized water; and (d) montmorillonite in 2 M NaCl brine.

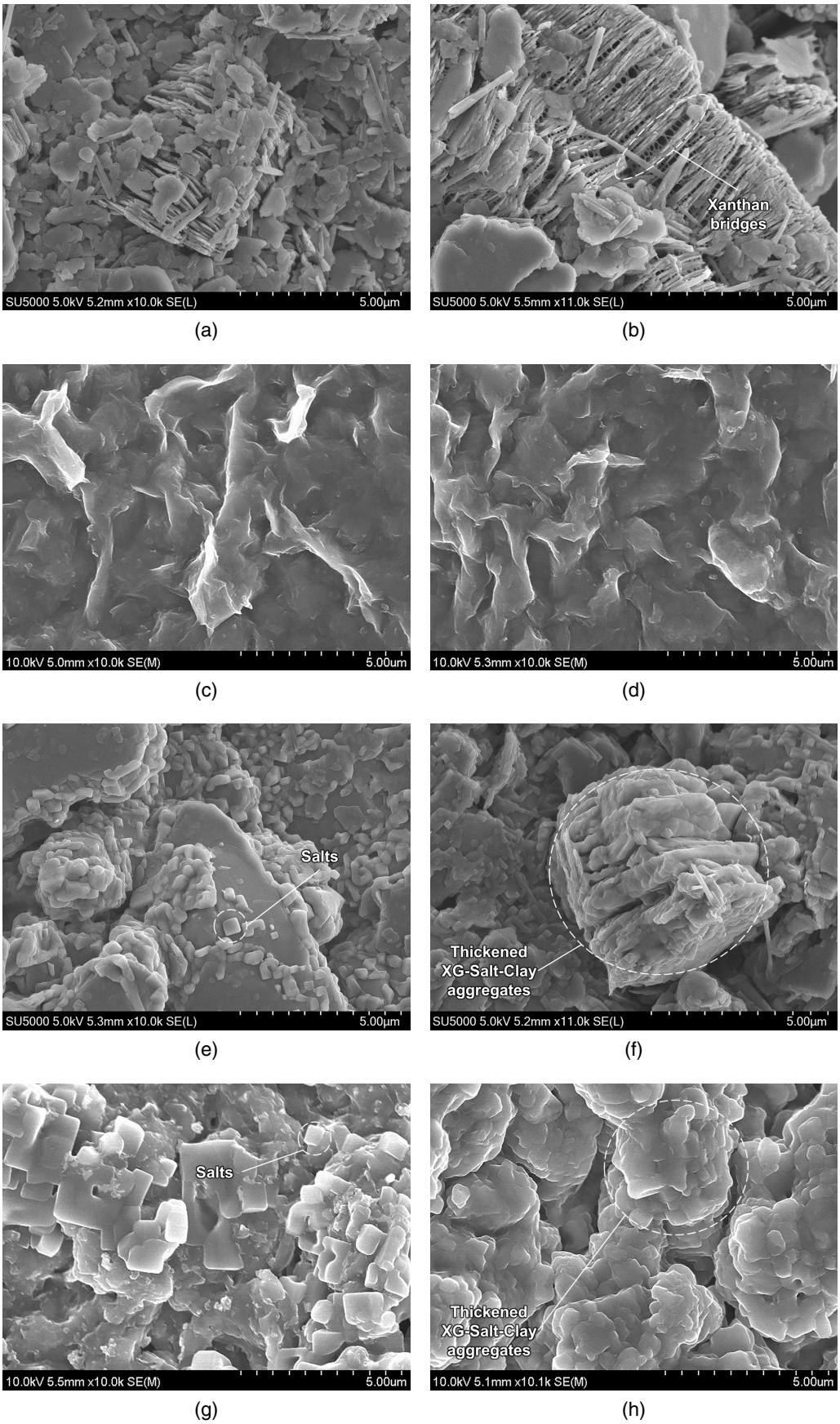

Fig. 4. SEM images of clay samples with different pore fluids and xanthan gum content: (a) untreated; and (b) 1% xanthan gum–treated kaolinite in deionized water; (c) untreated; and (d) 1% xanthan gum–treated montmorillonite in deionized water; (e) untreated; and (f) 1% xanthan gum–treated kaolinite in 2 M NaCl brine; (g) untreated; and (h) 1% xanthan gum–treated montmorillonite in 2 M NaCl brine.

for kerosene are not presented owing to the difficulties in obtaining the PL for the clay–kerosene mixtures (Kaya and Fang 2000). Both clays showed single $s_u - \mathrm{LI}$ relationships regardless of the presence of XG (Fig. 3). Therefore, the s_u of the XG-treated clays can be predicted using the LI assessed in the laboratory.

The obtained R parameter for kaolinite in DI water [$R = 24.26$; Fig. 3(a)] is in accordance with a previous study, showing that R values of kaolinite range between 11 and 47 (Vardanega and Haigh 2014). However, the R value of montmorillonite in DI water [$R = 12.54$; Fig. 3(c)] is significantly lower than the value of 100 suggested by Wood (1990); particularly, it is close to the values of 15–20 reported previously by Vardanega and Haigh (2014). In brine, the R value of kaolinite [Fig. 3(c)] and montmorillonite [Fig. 3(d)] decreased to 13.44 and 7.69, respectively, indicating a reduction in soil activity (plasticity) due to salt-induced double-layer compression.

SEM Analysis of XG Behavior

Fig. 4 shows SEM images of the untreated ($m_b/m_s = 0\%$) and XG-treated ($m_b/m_s = 1\%$) clays. The presented SEM images were obtained after drying; thus, the drying process itself may have influenced the morphology of the observed clay specimens in Fig. 4. Rigid crystalline particles were observed for kaolinite [Figs. 4(a and b)], whereas montmorillonite exhibited undulated flexible sheets [Figs. 4(c and d)]. This morphological difference was owing to the strong hydrogen bonds formed between the kaolinite sheets (Żbik et al. 2010; Au and Leong 2016). The untreated kaolinite in DI water showed random face-to-face, edge-to-edge, and edge-to-face structures [Fig. 4(a)], whereas XG-induced face-to-face aggregates were observed for $m_b/m_s = 1\%$ [Fig. 4(b)]. On the contrary, montmorillonite in DI water did not show distinctive structural variations following the XG treatment [Figs. 4(c and d)].

Precipitated salt crystals, which may have existed as dissolved ions during the experimental processes, were observed on the surfaces of the clays in 2-M-NaCl brine [Figs. 4(e and g)]. Salt crystals were less frequently observed in the XG-treated kaolinite with 2-M-NaCl brine [Fig. 4(f)] than in untreated kaolinite [Fig. 4(e)]. Unlike the 1%-XG-treated montmorillonite in DI water [Fig. 4(d)], the XG-treated montmorillonite in 2-M-NaCl brine showed well-developed aggregates [Fig. 4(h)]. This morphological difference could help explaining the observed increase in s_u with m_b/m_s increase for both clays in 2-M-NaCl brine solutions.

Conclusion

In this study, we assessed the s_u of XG-treated clays upon considering the pore–fluid chemistry and clay mineral effect. Montmorillonite showed the highest s_u, which favors the formation of viscous double layers in DI water, followed by brine and kerosene. In contrast, kaolinite showed the highest s_u with kerosene, followed by DI water and brine, indicating the influence of interparticle attraction forces on the s_u of kaolinite clay.

The XG treatment altered the s_u of the clays in terms of pore–fluid viscosity variation and XG-induced clay-particle aggregation. In DI, XG showed the maximum undrained shear strength with 0.5% m_b/m_s; the dominant effect of XG changed from viscosity enhancement to particle aggregation. At $m_b/m_s = 0.5\%$, the shear parameters α and β of XG increased by approximately 50% and 70%, respectively. In contrast, the XG-induced particle aggregation decreased the s_u of montmorillonite clay gradually. The parameters α and β showed 16% and 11% decrements with 2% XG as compared to those of untreated montmorillonite, respectively. In 2-M-NaCl brine, XG increased the s_u of both clays owing to water absorption and interaction with the salt ions, thereby showing increments of 46% and 74% in α and β, respectively. In kerosene, which is non-polar, XG did not affect the s_u of the two clays, indicating that hydrogel hydration is a prerequisite for XG treatment of clays. Kaolinite showed a higher R value than montmorillonite in DI. Moreover, both clays showed higher R values in DI than in brine. Meanwhile, the XG treatment had no effect on the R values.

Overall, the XG treatment was effective in increasing the shear strength of the clays in the undrained state, especially in high-salinity conditions. The optimal XG content and mineral properties must be considered to use XG in treating soils with low salinity (e.g., riverbeds). Nevertheless, to add XG to soils surrounded by low-permittivity pore fluids, such as in oil fields, XG gelation must be performed prior to soil treatment. In future studies, the water absorption capabilities of kaolinite, montmorillonite, and XG should be compared.

Data Availability Statement

All data, models, and code generated or used during the study are present in the published article.

Acknowledgments

This study was financially supported by the Water Management Research Program funded by the Ministry of Land, Infrastructure, and Transport (MOLIT) of the Korean Government (21AWMP-B114119-06) and the New Faculty Research Fund of Ajou University.

Notation

The following symbols are used in this paper:

d = penetration depth (mm);
K = cone factor;
LI = liquidity index, $(w-\mathrm{PL})/(\mathrm{LL}-\mathrm{PL})$;
LL = liquid limit (%);
m_b/m_s = XG-to-soil mass ratio (%);
PL = plastic limit (%);
R = strength gain factor (ratio of undrained shear strength at PL and LL);
SSA = specific surface area (m^2/g);
s_u = undrained shear strength (kPa);
s_u^{FC} = undrained shear strength evaluated through fall cone test (kPa);
s_u^{LL} = undrained shear strength at LL (kPa);
s_u^{PL} = undrained shear strength at PL (kPa);
s_u^{V} = undrained shear strength evaluated through laboratory vane shear test (kPa);
W = weight of cone (g);
w = water content (%);
XG = xanthan gum biopolymer;
α = water content when $s_u = 1\,\mathrm{kPa}$ (%); and
β = variation of $\log s_u$ with $\log w$.

References

Anirudhan, T. S., and M. Ramachandran. 2007. "Surfactant-modified bentonite as adsorbent for the removal of humic acid from wastewaters."

Appl. Clay Sci. 35 (3): 276–281. https://doi.org/10.1016/j.clay.2006.09.009.

ASTM. 2016. *Standard test methods for laboratory miniature vane shear test for saturated fine-grained clayey soil*. ASTM D4648/D4648M-16. West Conshohocken, PA: ASTM.

ASTM. 2017. *Standard test methods for liquid limit, plastic limit, and plasticity index of soils*. ASTM D4318-17. West Conshohocken, PA: ASTM.

ASTM. 2019. *Standard test methods for laboratory determination of water (moisture) content of soil and rock by mass*. ASTM D2216-19. West Conshohocken, PA: ASTM.

Au, P.-I., and Y.-K. Leong. 2016. "Surface chemistry and rheology of slurries of kaolinite and montmorillonite from different sources." *KONA Powder Part. J.* 33 (6): 17–32. https://doi.org/10.14356/kona.2016007.

Bouazza, A., W. Gates, and P. Ranjith. 2009. "Hydraulic conductivity of biopolymer-treated silty sand." *Géotechnique* 59 (1): 71–72. https://doi.org/10.1680/geot.2007.00137.

British Standards Institution. 2017. *BS EN ISO 17892: Geotechnical investigation and testing—Laboratory testing of soil. Part 6: Fall cone test*. London: British Standards Institution.

Cabalar, A. F., M. Wiszniewski, and Z. Skutnik. 2017. "Effects of xanthan gum biopolymer on the permeability, odometer, unconfined compressive and triaxial shear behavior of a sand." *Soil Mech. Found. Eng.* 54 (5): 356–361. https://doi.org/10.1007/s11204-017-9481-1.

Cao, S. C., J. Jang, J. Jung, W. F. Waite, T. S. Collett, and P. Kumar. 2019. "2D micromodel study of clogging behavior of fine-grained particles associated with gas hydrate production in NGHP-02 gas hydrate reservoir sediments." *Mar. Pet. Geol.* 108 (Oct): 714–730. https://doi.org/10.1016/j.marpetgeo.2018.09.010.

Carrier, B., L. Wang, M. Vandamme, R. J. M. Pellenq, M. Bornert, A. Tanguy, and H. Van Damme. 2013. "ESEM study of the humidity-induced swelling of clay film." *Langmuir* 29 (41): 12823–12833. https://doi.org/10.1021/la402781p.

Chang, I., and G.-C. Cho. 2019. "Shear strength behavior and parameters of microbial gellan gum-treated soils: From sand to clay." *Acta Geotech.* 14 (2): 361–375. https://doi.org/10.1007/s11440-018-0641-x.

Chang, I., J. Im, and G.-C. Cho. 2016a. "Geotechnical engineering behaviors of gellan gum biopolymer treated sand." *Can. Geotech. J.* 53 (10): 1658–1670. https://doi.org/10.1139/cgj-2015-0475.

Chang, I., J. Im, and G. C. Cho. 2016b. "Introduction of microbial biopolymers in soil treatment for future environmentally-friendly and sustainable geotechnical engineering." *Sustainability* 8 (3): 251. https://doi.org/10.3390/su8030251.

Chang, I., J. Im, A. K. Prasidhi, and G.-C. Cho. 2015. "Effects of xanthan gum biopolymer on soil strengthening." *Constr. Build. Mater.* 74 (Jan): 65–72. https://doi.org/10.1016/j.conbuildmat.2014.10.026.

Chang, I., Y.-M. Kwon, J. Im, and G.-C. Cho. 2019. "Soil consistency and interparticle characteristics of xanthan gum biopolymer-containing soils with pore-fluid variation." *Can. Geotech. J.* 56 (8): 1206–1213. https://doi.org/10.1139/cgj-2018-0254.

Chang, I., M. Lee, A. T. P. Tran, S. Lee, Y.-M. Kwon, J. Im, and G.-C. Cho. 2020. "Review on biopolymer-based soil treatment (BPST) technology in geotechnical engineering practices." *Transp. Geotech.* 24 (Sep): 100385. https://doi.org/10.1016/j.trgeo.2020.100385.

Chen, C., L. Wu, and M. Harbottle. 2019a. "Exploring the effect of biopolymers in near-surface soils using xanthan gum–modified sand under shear." *Can. Geotech. J.* 57 (8): 1–10. https://doi.org/10.1139/cgj-2019-0284.

Chen, C., L. Wu, M. Perdjon, X. Huang, and Y. Peng. 2019b. "The drying effect on xanthan gum biopolymer treated sandy soil shear strength." *Constr. Build. Mater.* 197 (Feb): 271–279. https://doi.org/10.1016/j.conbuildmat.2018.11.120.

Chen, X., and Y. Peng. 2018. "Managing clay minerals in froth flotation—A critical review." *Miner. Process. Extr. Metall. Rev.* 39 (5): 289–307. https://doi.org/10.1080/08827508.2018.1433175.

Chenu, C., and J. Guérif. 1991. "Mechanical strength of clay minerals as influenced by an adsorbed polysaccharide." *Soil Sci. Soc. Am. J.* 55 (4): 1076–1080. https://doi.org/10.2136/sssaj1991.03615995005500040030x.

Chow, S., F. Alonso-Marroquin, and D. Airey. 2012. "Viscous rate effects in shear strength of clay." In *Proc., 11th Australia–New Zealand Conf. on Geomechanics*, 15–18. Saint Ives, NSW, Australia: Australian Geomechanics Society.

Dehghan, H., A. Tabarsa, N. Latifi, and Y. Bagheri. 2019. "Use of xanthan and guar gums in soil strengthening." *Clean Technol. Environ. Policy* 21 (1): 155–165. https://doi.org/10.1007/s10098-018-1625-0.

Doi, A., M. Ejtemaei, and A. V. Nguyen. 2019. "Effects of ion specificity on the surface electrical properties of kaolinite and montmorillonite." *Miner. Eng.* 143 (Nov): 105929. https://doi.org/10.1016/j.mineng.2019.105929.

Dolinar, B., and L. Trauner. 2007. "The impact of structure on the undrained shear strength of cohesive soils." *Eng. Geol.* 92 (1): 88–96. https://doi.org/10.1016/j.enggeo.2007.04.003.

Dontsova, K. M., and J. M. Bigham. 2005. "Anionic polysaccharide sorption by clay minerals." *Soil Sci. Soc. Am. J.* 69 (4): 1026–1035. https://doi.org/10.2136/sssaj2004.0203.

Du, J., R. A. Pushkarova, and R. S. C. Smart. 2009. "A cryo-SEM study of aggregate and floc structure changes during clay settling and raking processes." *Int. J. Miner. Process.* 93 (1): 66–72. https://doi.org/10.1016/j.minpro.2009.06.004.

Dukhin, A. S., and P. J. Goetz. 2010. *Characterization of liquids, nano-and microparticulates, and porous bodies using ultrasound*. Oxford, UK: Elsevier.

Espinoza, D. N., and J. C. Santamarina. 2012. "Clay interaction with liquid and supercritical CO_2: The relevance of electrical and capillary forces." *Int. J. Greenhouse Gas Control* 10 (Sep): 351–362. https://doi.org/10.1016/j.ijggc.2012.06.020.

García-Ochoa, F., V. E. Santos, J. A. Casas, and E. Gómez. 2000. "Xanthan gum: Production, recovery, and properties." *Biotechnol. Adv.* 18 (7): 549–579. https://doi.org/10.1016/S0734-9750(00)00050-1.

Giese, R. F. 2003. "Kaolin group minerals." In *Encyclopedia of sediments and sedimentary rocks*, edited by G. V. Middleton, M. J. Church, M. Coniglio, L. A. Hardie, and F. J. Longstaffe, 398–400. Berlin: Springer.

Guo, J., and X. Wen. 2020. "Performances and mechanisms of sludge dewatering by a biopolymer from piggery wastewater and application of the dewatered sludge in remediation of Cr(VI)-contaminated soil." *J. Environ. Manage.* 259 (Apr): 109678. https://doi.org/10.1016/j.jenvman.2019.109678.

Gutierrez, M., R. Nygård, K. Høeg, and T. Berre. 2008. "Normalized undrained shear strength of clay shales." *Eng. Geol.* 99 (1): 31–39. https://doi.org/10.1016/j.enggeo.2008.02.002.

Ham, S.-M., I. Chang, D.-H. Noh, T.-H. Kwon, and B. Muhunthan. 2018. "Improvement of surface erosion resistance of sand by microbial biopolymer formation." *J. Geotech. Geoenviron. Eng.* 144 (7): 06018004. https://doi.org/10.1061/(ASCE)GT.1943-5606.0001900.

Hassler, R. A., and D. H. Doherty. 1990. "Genetic engineering of polysaccharide structure: Production of variants of xanthan gum in *Xanthomonas campestris*." *Biotechnol. Progr.* 6 (3): 182–187. https://doi.org/10.1021/bp00003a003.

Hemar, Y., M. Tamehana, P. A. Munro, and H. Singh. 2001. "Influence of xanthan gum on the formation and stability of sodium caseinate oil-in-water emulsions." *Food Hydrocolloids* 15 (4): 513–519. https://doi.org/10.1016/S0268-005X(01)00075-3.

Hong, Z.-S., X. Bian, Y.-J. Cui, Y.-F. Gao, and L.-L. Zeng. 2013. "Effect of initial water content on undrained shear behaviour of reconstituted clays." *Géotechnique* 63 (6): 441–450. https://doi.org/10.1680/geot.11.P.114.

Hyde, A. F. L., and S. J. Ward. 1986. "The effect of cyclic loading on the undrained shear strength of a silty clay." *Mar. Geotechnol.* 6 (3): 299–314. https://doi.org/10.1080/10641198609388192.

Inglethorpe, S. D. J., D. J. Morgan, D. E. Highley, and A. J. Bloodworth. 1993. *Industrial minerals laboratory manual: Bentonite*. Nottingham, UK: British Geological Survey.

Jang, J., and J. C. Santamarina. 2016. "Fines classification based on sensitivity to pore-fluid chemistry." *J. Geotech. Geoenviron. Eng.* 142 (4): 06015018. https://doi.org/10.1061/(ASCE)GT.1943-5606.0001420.

Kang, J., and R. A. McLaughlin. 2020. "Polyacrylamide and chitosan biopolymer for flocculation and turbidity reduction in soil suspensions." *J. Polym. Environ.* 28 (4): 1335–1343. https://doi.org/10.1007/s10924-020-01682-2.

Katzbauer, B. 1998. "Properties and applications of xanthan gum." *Polym. Degrad. Stab.* 59 (1): 81–84. https://doi.org/10.1016/S0141-3910(97)00180-8.

Kaya, A., and H.-Y. Fang. 2000. "The effects of organic fluids on physicochemical parameters of fine-grained soils." *Can. Geotech. J.* 37 (5): 943–950. https://doi.org/10.1139/t00-023.

Kayabali, K., and O. O. Tufenkci. 2010. "Shear strength of remolded soils at consistency limits." *Can. Geotech. J.* 47 (3): 259–266. https://doi.org/10.1139/T09-095.

Khachatoorian, R., I. G. Petrisor, C.-C. Kwan, and T. F. Yen. 2003. "Biopolymer plugging effect: Laboratory-pressurized pumping flow studies." *J. Petrol. Sci. Eng.* 38 (1): 13–21. https://doi.org/10.1016/S0920-4105(03)00019-6.

Khatami, H. R., and B. C. O'Kelly. 2012. "Improving mechanical properties of sand using biopolymers." *J. Geotech. Geoenviron. Eng.* 139 (8): 1402–1406. https://doi.org/10.1061/(ASCE)GT.1943-5606.0000861.

Koumoto, T., and G. T. Houlsby. 2001. "Theory and practice of the fall cone test." *Géotechnique* 51 (8): 701–712. https://doi.org/10.1680/geot.2001.51.8.701.

Kulhawy, F. H., and P. W. Mayne. 1990. *Manual on estimating soil properties for foundation design*. New York: Electric Power Research Institute.

Kwon, Y.-M., I. Chang, M. Lee, and G.-C. Cho. 2019. "Geotechnical engineering behaviors of biopolymer-treated soft marine soil." *Geomech. Eng.* 17 (5): 453–464. https://doi.org/10.12989/gae.2019.17.5.453.

Kwon, Y.-M., S.-M. Ham, T.-H. Kwon, G.-C. Cho, and I. Chang. 2020. "Surface-erosion behaviour of biopolymer-treated soils assessed by EFA." *Géotech. Lett.* 10 (2): 1–7. https://doi.org/10.1680/jgele.19.00106.

Kwon, Y.-M., J. Im, I. Chang, and G.-C. Cho. 2017. "ε-polylysine biopolymer for coagulation of clay suspensions." *Geomech. Eng.* 12 (5): 753–770. https://doi.org/10.12989/gae.2017.12.5.753.

Laird, D. A. 1997. "Bonding between polyacrylamide and clay mineral surfaces." *Soil Sci.* 162 (11): 826–832. https://doi.org/10.1097/00010694-199711000-00006.

Latifi, N., S. Horpibulsuk, C. L. Meehan, M. Z. A. Majid, M. M. Tahir, and E. T. Mohamad. 2017. "Improvement of problematic soils with biopolymer—An environmentally friendly soil stabilizer." *J. Mater. Civ. Eng.* 29 (2): 04016204. https://doi.org/10.1061/(ASCE)MT.1943-5533.0001706.

Lee, S., I. Chang, M.-K. Chung, Y. Kim, and J. Kee. 2017. "Geotechnical shear behavior of xanthan gum biopolymer treated sand from direct shear testing." *Geomech. Eng.* 12 (5): 831–847. https://doi.org/10.12989/gae.2017.12.5.831.

Lee, S., M. Chung, H. M. Park, K.-I. Song, and I. Chang. 2019. "Xanthan gum biopolymer as soil-stabilization binder for road construction using local soil in Sri Lanka." *J. Mater. Civ. Eng.* 31 (11): 06019012. https://doi.org/10.1061/(ASCE)MT.1943-5533.0002909.

Liu, X., X. Lu, R. Wang, E. J. Meijer, H. Zhou, and H. He. 2012. "Atomic scale structures of interfaces between kaolinite edges and water." *Geochim. Cosmochim. Acta* 92 (2): 233–242. https://doi.org/10.1016/j.gca.2012.06.008.

Malik, M., and J. Letey. 1991. "Adsorption of polyacrylamide and polysaccharide polymers on soil materials." *Soil Sci. Soc. Am. J.* 55 (2): 380–383. https://doi.org/10.2136/sssaj1991.03615995005500020014x.

Mayne, P. W. 1985. "Stress anisotropy effects on clay strength." *J. Geotech. Eng.* 111 (3): 356–366. https://doi.org/10.1061/(ASCE)0733-9410(1985)111:3(356).

Milas, M., M. Rinaudo, and B. Tinland. 1985. "The viscosity dependence on concentration, molecular weight and shear rate of xanthan solutions." *Polym. Bull.* 14 (2): 157–164. https://doi.org/10.1007/BF00708475.

Mitchell, J. K., and K. Soga. 2005. *Fundamentals of soil behavior*. Hoboken, NJ: Wiley.

Nugent, R. A., G. Zhang, and R. P. Gambrell. 2009. "Effect of exopolymers on the liquid limit of clays and its engineering implications." *Transp. Res. Rec.* 2101 (1): 34–43. https://doi.org/10.3141/2101-05.

O'Kelly, B. C., P. J. Vardanega, and S. K. Haigh. 2018. "Use of fall cones to determine Atterberg limits: A review." *Géotechnique* 68 (10): 843–856. https://doi.org/10.1680/jgeot.17.R.039.

Penner, D., and G. Lagaly. 2001. "Influence of anions on the rheological properties of clay mineral dispersions." *Appl. Clay Sci.* 19 (1): 131–142. https://doi.org/10.1016/S0169-1317(01)00052-7.

Petri, D. F. S. 2015. "Xanthan gum: A versatile biopolymer for biomedical and technological applications." *J. Appl. Polym. Sci.* 132 (23): 15. https://doi.org/10.1002/app.42035.

Rao, S. M., A. Sridharan, and M. R. Shenoy. 1993. "Influence of starch polysaccharide on the remoulded properties of two Indian clay samples." *Can. Geotech. J.* 30 (3): 550–553. https://doi.org/10.1139/t93-047.

Sachan, A., and D. Penumadu. 2007. "Effect of microfabric on shear behavior of kaolin clay." *J. Geotech. Geoenviron. Eng.* 133 (3): 306–318. https://doi.org/10.1061/(ASCE)1090-0241(2007)133:3(306).

Santamarina, J. C., K. A. Klein, and M. A. Fam. 2001. *Soils and waves*. Hoboken, NJ: Wiley.

Santamarina, J. C., K. A. Klein, Y. H. Wang, and E. Prencke. 2002. "Specific surface: Determination and relevance." *Can. Geotech. J.* 39 (1): 233–241. https://doi.org/10.1139/t01-077.

Schlue, B. F., T. Moerz, and S. Kreiter. 2010. "Influence of shear rate on undrained vane shear strength of organic harbor mud." *J. Geotech. Geoenviron. Eng.* 136 (10): 1437–1447. https://doi.org/10.1061/(ASCE)GT.1943-5606.0000356.

Secor, R. B., and C. J. Radke. 1985. "Spillover of the diffuse double layer on montmorillonite particles." *J. Colloid Interface Sci.* 103 (1): 237–244. https://doi.org/10.1016/0021-9797(85)90096-7.

Sharma, B., and K. Bora Padma. 2003. "Plastic limit, liquid limit and undrained shear strength of soil—Reappraisal." *J. Geotech. Geoenviron. Eng.* 129 (8): 774–777. https://doi.org/10.1061/(ASCE)1090-0241(2003)129:8(774).

Singh, S. P., and R. Das. 2020. "Geo-engineering properties of expansive soil treated with xanthan gum biopolymer." *Geomech. Geoeng.* 15 (2): 107–122. https://doi.org/10.1080/17486025.2019.1632495.

Soldo, A., M. Miletić, and M. L. Auad. 2020. "Biopolymers as a sustainable solution for the enhancement of soil mechanical properties." *Sci. Rep.* 10 (1): 267. https://doi.org/10.1038/s41598-019-57135-x.

Spagnoli, G., T. Fernández-Steeger, M. Feinendegen, H. Stanjek, and R. Azzam. 2010. "The influence of the dielectric constant and electrolyte concentration of the pore fluids on the undrained shear strength of smectite." *Soils Found.* 50 (5): 757–763. https://doi.org/10.3208/sandf.50.757.

Sridharan, A., and K. Prakash. 1999. "Mechanisms controlling the undrained shear strength behaviour of clays." *Can. Geotech. J.* 36 (6): 1030–1038. https://doi.org/10.1139/t99-071.

Sridharan, A., and G. V. Rao. 1979. "Shear strength behaviour of saturated clays and the role of the effective stress concept." *Géotechnique* 29 (2): 177–193. https://doi.org/10.1680/geot.1979.29.2.177.

Stone, K. J. L., and K. D. Phan. 1995. "Cone penetration tests near the plastic limit." *Géotechnique* 45 (1): 155–158. https://doi.org/10.1680/geot.1995.45.1.155.

Sujatha, E. R., S. Atchaya, A. Sivasaran, and R. S. Keerdthe. 2020. "Enhancing the geotechnical properties of soil using xanthan gum—An eco-friendly alternative to traditional stabilizers." *Bull. Eng. Geol. Environ.* 80 (2): 1157–1167. https://doi.org/10.1007/s10064-020-02010-7.

Tombácz, E., and M. Szekeres. 2006. "Surface charge heterogeneity of kaolinite in aqueous suspension in comparison with montmorillonite." *Appl. Clay Sci.* 34 (1): 105–124. https://doi.org/10.1016/j.clay.2006.05.009.

Trauner, L., B. Dolinar, and M. Mišič. 2005. "Relationship between the undrained shear strength, water content, and mineralogical properties of fine-grained soils." *Int. J. Geomech.* 5 (4): 350–355. https://doi.org/10.1061/(ASCE)1532-3641(2005)5:4(350).

Turkoz, E., A. Perazzo, C. B. Arnold, and H. A. Stone. 2018. "Salt type and concentration affect the viscoelasticity of polyelectrolyte solutions." *Appl. Phys. Lett.* 112 (20): 203701. https://doi.org/10.1063/1.5026573.

Vardanega, P. J., and S. K. Haigh. 2014. "The undrained strength–liquidity index relationship." *Can. Geotech. J.* 51 (9): 1073–1086. https://doi.org/10.1139/cgj-2013-0169.

Villanueva, M. P., L. Cabedo, J. M. Lagarón, and E. Giménez. 2010. "Comparative study of nanocomposites of polyolefin compatibilizers containing kaolinite and montmorillonite organoclays." *J. Appl. Polym. Sci.* 115 (3): 1325–1335. https://doi.org/10.1002/app.30278.

Wan, J., and T. K. Tokunaga. 2002. "Partitioning of clay colloids at air–water interfaces." *J. Colloid Interface Sci.* 247 (1): 54–61. https://doi.org/10.1006/jcis.2001.8132.

Wang, Y. H., and W. K. Siu. 2006. "Structure characteristics and mechanical properties of kaolinite soils. I. Surface charges and structural characterizations." *Can. Geotech. J.* 43 (6): 587–600. https://doi.org/10.1139/t06-026.

Warkentin, B. P., and R. N. Yong. 1962. "Shear strength of montmorillonite and kaolinite related to interparticle forces." In *Clays and clay minerals*, edited by E. Ingerson, 210–218. İzmir, Turkey: Pergamon.

Wood, D. M. 1990. *Soil behaviour and critical state soil mechanics*. Cambridge, MA: Cambridge University Press.

Wroth, C. P., and D. M. Wood. 1978. "The correlation of index properties with some basic engineering properties of soils." *Can. Geotech. J.* 15 (2): 137–145. https://doi.org/10.1139/t78-014.

Żbik, M. S., N. A. Raftery, R. S. C. Smart, and R. L. Frost. 2010. "Kaolinite platelet orientation for XRD and AFM applications." *Appl. Clay Sci.* 50 (3): 299–304. https://doi.org/10.1016/j.clay.2010.08.010.

Zhou, C., P. S. So, and X. W. Chen. 2020. "A water retention model considering biopolymer–soil interactions." *J. Hydrol.* 586 (Jul): 124874. https://doi.org/10.1016/j.jhydrol.2020.124874.